

Fast Learning in Quantitative Finance with Extreme Learning Machine

Liexin Cheng[†], Xue Cheng^{‡*}, and Shuaiqiang Liu[§]

May 25, 2025

[†] School of Mathematical Science, Peking University, Beijing, China

[‡] School of Mathematical Science, Peking University, Beijing, China

[§] Delft Institute of Applied Mathematics, Delft University of Technology, Netherlands

Abstract

This paper demonstrates that a broad class of problems in quantitative finance, including those previously addressed using deep neural networks, can be efficiently solved using single-layer neural networks without iterative gradient-based training, namely extreme learning machine (ELM). ELM utilizes a single-layer network with randomly initialized hidden nodes and analytically computed output weights obtained via convex optimization, enabling rapid training and inference. Both supervised and unsupervised learning tasks are explored.

In supervised learning, ELM is employed to learn parametric option pricing functions, predict intraday stock returns, and complete implied volatility surfaces. Compared with deep neural networks, Gaussian process regression, and logistic regression, ELM achieves higher computational speed, comparable accuracy, and superior generalization.

In unsupervised learning, ELM numerically solves Black-Scholes-type PDEs, and outperforms Physics-Informed Neural Networks in training speed without losing precision. The approximation and generalization abilities of ELM are briefly discussed.

The findings establish ELM as a practical and efficient tool for various tasks in quantitative finance.

1 Introduction

Machine learning methods, such as logistic regression (LR), Gaussian process regression (GPR, see [Williams and Rasmussen \(1995\)](#)), and artificial neural network (ANN, see [Wu](#)

*Corresponding author. Email: chengxue@math.pku.edu.cn

and Feng (2018)), have emerged as transformative tools in quantitative finance that address complex challenges such as option pricing, risk management, and high-dimensional data analysis. Their ability to approximate nonlinear functions and process vast datasets has positioned them as alternatives to traditional numerical methods. For instance, in the field of option pricing and hedging, see a review Ruf and Wang (2020), deep neural networks are employed to either speed up solving related mathematical models (e.g., calibration neural networks (Liu et al. (2019)), deep learning volatility (Horvath et al. (2021)), among others) or overcome the curse of dimensionality for high dimensional problems (e.g., Physics-informed neural networks (PINN) (Raissi et al. (2019)), Deep BSDE (Han et al. (2018)), Deep backward dynamic programming (Hur   et al. (2020)), Deep Galerkin Method (Sirignano and Spiliopoulos (2018)), as well as many other variants). On the other hand, machine learning methods, such as LR, GPR or recently deep learning, are applied to extract insights and predict trends from historical financial data.

We demonstrate that a broad class of problems in quantitative finance, previously addressed using deep neural network-based methods, can be efficiently solved using single hidden-layer neural networks, i.e., Extreme Learning Machine (ELM).

Introduced by Huang et al. (2006b), ELMs offer a compelling alternative to traditional deep neural networks (DNNs) by addressing the critical limitations inherent in DNN-based approaches. DNNs rely on computationally intensive nonconvex optimization via gradient-based methods like stochastic gradient descent (SGD), a process prone to local minima and sequential layer dependencies. In comparison, ELM employs a single-hidden-layer architecture with randomly initialized hidden weights and analytically solved output weights through linear least squares. This framework transforms training into a convex optimization problem, which guarantees convergence while avoiding iterative backpropagation. Consequently, ELM usually achieves an order-of-magnitude faster training process. With respect to inference speed, ELM also prevails since a single hidden-layer network can be efficiently implemented through parallel computing, unlike DNNs in which the next layer has to wait for the output of the previous layer. Moreover, ELM retains the universal approximation capabilities of DNNs (Neufeld and Schmocker (2023)). Although ELM has shown success in many fields of research as reviewed in Wang et al. (2022), their potential in finance, particularly for derivative pricing and financial applications, remains underexplored.

This work bridges the gap between ELM theory and financial practice by demonstrating its efficacy in the supervised and unsupervised learning paradigms.

In supervised learning, the process typically involves two key phases: an initial offline training stage followed by frequent online inference operations. Since the training phase is generally performed once, the efficacy of inference is particularly beneficial to the application of the ANN-based method such as option pricing and model calibration (e.g., Horvath et al. (2021), Liu et al. (2019)). We will show that ELM can outperform DNNs in terms of model inference by taking stochastic volatility models as an example. Beyond inference speed, ELM is also shown to exhibit favorable generalization characteristics compared to GPR and LR, effectively balancing accuracy with computational efficiency. Regarding training, supervised learning tasks may not inherently require rapid

training, but there are many scenarios where fast training is critical. For example, when model inference necessarily depends on incremental data information (e.g., predicting financial time series), training needs to be performed frequently with updated data. In the following, we list some typical scenarios that will be experimented with in the paper:

1. learning the pricing function of stochastic volatility models,
2. real-time predicting stock returns in high frequency data,
3. completing implied volatility surfaces over several consecutive months.

By means of unsupervised learning, solving multidimensional PDEs requires two pillars, overcoming the curse of dimensionality and fast training. Traditional numerical methods such as finite difference, finite element, and volume approaches face the challenge of curse of dimensionality. While ANNs have emerged as a promising alternative to overcome this limitation, their practical implementation often requires computationally efficient training procedures. ELM offers a compelling solution in this context via their ability to solve option pricing functions while effectively circumventing dimensional constraints, as evidenced by their successful application to Black-Scholes-type PDEs in [Gonon \(2023\)](#), which proves that ELM can overcome the curse of dimensionality, and rough volatility models ([Jacquier and Zuric \(2023\)](#)). Building on these advantages, our work advances the field by incorporating ELM within the PINN framework in financial PDEs, which demonstrates the strength of ELM in achieving substantially faster training compared to DNN.

The remainder of this paper is organized as follows. Section 2 outlines the theoretical foundations of ELM, including the original ELM and its enhanced variants. Section 3 explores supervised learning applications, focusing on inference speed, incremental training, and comparative performance against DNNs, GPR and LR. Section 4 discusses unsupervised learning via ELM-based PINNs, emphasizing their role in solving multidimensional financial PDEs. Section 5 concludes.

2 Theory of ELM

2.1 ELM

An ELM is a single hidden layer feed-forward neural network whose hidden-layer weights are randomly generated before the training process. ELM can be trained quite efficiently for both classification and regression problems. The training of ELM solves a least-square problem instead of gradient-descent algorithms in traditional neural networks. The following summarizes:

Given a set of training data $(\mathbf{x}_j, y_j), j = 1, 2, \dots, N$, where $\mathbf{x}_j \in \mathbf{R}^d$ and $y_j \in \mathbf{R}$, the output function of ELM is

$$\text{ELM}(\mathbf{x}_j) := f_L(\mathbf{x}_j) = \sum_{i=1}^L \beta_i G(\mathbf{w}_i \cdot \mathbf{x}_j + b_i), \quad j = 1, 2, \dots, N, \quad (1)$$

where $f_L : \mathbf{R}^d \rightarrow \mathbf{R}$, L is the number of hidden neurons, $G(\cdot)$ is an activation function, $\mathbf{w}_i \in \mathbf{R}^d$ is the weight vector that connects the input layer to the i th hidden node and $b_i \in \mathbf{R}$ is the bias of the hidden node. The weights and biases (\mathbf{w}_i, b_i) are generated independently and randomly from a continuous distribution $D \in \mathbf{R}^{L+1}$. We also write the N equations (1) compactly as:

$$\mathbf{H} \cdot \boldsymbol{\beta} = \mathbf{Y}, \quad (2)$$

where $\mathbf{H} \in \mathbf{R}^{N \times L}$ is the hidden layer output matrix with the (j, i) term $G(\mathbf{w}_i \cdot \mathbf{x}_j + b_j)$, $\boldsymbol{\beta} = [\beta_1, \dots, \beta_L]^\top$ and $\mathbf{Y} = [y_1, \dots, y_N]^\top$.

The least square solution of the linear equation system is

$$\boldsymbol{\beta} = \mathbf{H}^\dagger \mathbf{Y},$$

where \mathbf{H}^\dagger is the generalized Moore-Penrose inverse of matrix \mathbf{H} . It has been show in [Huang et al. \(2006b\)](#) that H is of full column rank with probability one, under mild conditions of the neural network. Then, if $L \leq N$, we take $\mathbf{H}^\dagger = (\mathbf{H}^\top \mathbf{H})^{-1} \mathbf{H}^\top$, in which case a Cholesky decomposition with complexity $O(L^3)$ can be applied to solve $\boldsymbol{\beta}$. In more general cases where H is rank deficient, the singular value decomposition can be used with numerical stability. Moreover, for large sparse situations, iterative methods such as conjugate gradient or GMRES can be more efficient.

It was also shown in [Huang et al. \(2006a\)](#) that given any positive value $\epsilon > 0$, we can find an $L \leq N$ such that $\|\mathbf{H}\boldsymbol{\beta} - \mathbf{Y}\|_2 < \epsilon$ under mild network structure assumptions. One can also add a regularization term in the solution by minimizing $\|\mathbf{H} \cdot \boldsymbol{\beta} - \mathbf{Y}\|_2^2 + C\|\boldsymbol{\beta}\|_2^2$, which results in

$$\boldsymbol{\beta} = (\mathbf{H}^\top \mathbf{H} + C\mathbf{I})^{-1} \mathbf{H}^\top \mathbf{Y}, \quad (3)$$

where C is a constant that determines the degree of regularization. Unlike conventional feedforward networks, ELM results in a convex optimization problem.

2.2 Incremental ELM

Following the baseline ELM (cf. [Huang et al. \(2006b\)](#)), incremental ELM methods were proposed to automatically determine network architectures given an application scenario. I-ELM by [Huang et al. \(2006a\)](#) adds randomly generated nodes to the hidden layer one by one and fixes the output weights of the existing hidden nodes when a new hidden node was added. As an improvement to I-ELM, CI-ELM ([Huang and Chen \(2007\)](#)) recalculated the entire output weights every time a new hidden node is added, which yields faster error convergence in various datasets while keeping the simplicity of I-ELM. That is, the reduction in testing RMSE as the number of hidden nodes increases becomes faster in CI-ELM than in I-ELM. Later, [Feng et al. \(2009\)](#) proposed EM-ELM that increases nodes one by one or group by group based on error-minimization criteria. EM-ELM was shown to achieve even faster convergence rates and reduced computational complexity.

In Xu et al. (2016), an improved EM-ELM algorithm, called Enhanced Incremental Regularized ELM (EIR-ELM), was developed. Compared with EM-ELM, the new algorithm achieved better generalization performance by introducing regularization method and by selecting hidden nodes to be added to the network. The implementation of the EIR-ELM algorithm is summarized below.

For a given training data set $\aleph = \{(\mathbf{x}_i, \mathbf{t}_i) \mid \mathbf{x}_i \in \mathbf{R}^n, \mathbf{t}_i \in \mathbf{R}^m, i = 1, \dots, N\}$, the initial number of hidden nodes N_0 , the maximum number of hidden nodes N_{\max} and the expected learning accuracy ϵ :

I. Initialize the neural network:

1. Assign the input weights vectors \mathbf{w}_i and basis $b_i, i = 1, \dots, N_0$ randomly.
2. Calculate the hidden layer output matrix \mathbf{H}_0 .
3. Calculate the output weight $\beta_0, \beta_0 = \mathbf{D}_0 \mathbf{T} := (\mathbf{H}_0^T \mathbf{H}_0 + \mathbf{C} \mathbf{I})^{-1} \mathbf{H}_0^T \mathbf{T}$, where $\mathbf{T} = [\mathbf{t}_1, \dots, \mathbf{t}_N]^T$.
4. Let $s = N_0$, calculate the learning accuracy ϵ_s .

II. Update the network recursively. While $s < N_{\max}$ and $\epsilon_s < \epsilon$

1. Let $s = s + 1$.
2. For $i = 1 : k$
 - (a) Generate a new hidden node i randomly, $\mathbf{H}_s^i = [\mathbf{H}_{s-1}, \mathbf{v}_s^i]$
 - (b) Update the output weight as follows:

$$\mathbf{M}_s = \frac{\mathbf{v}_s^{iT} (\mathbf{I} - \mathbf{H}_{s-1} \mathbf{D}_{s-1})}{\mathbf{v}_s^{iT} (\mathbf{I} - \mathbf{H}_{s-1} \mathbf{D}_{s-1}) \mathbf{v}_s^i + \mathbf{C}}$$

$$\mathbf{L}_s = \mathbf{D}_{s-1} (\mathbf{I} - \mathbf{v}_s^i \mathbf{M}_s), \quad \beta_s^i = \mathbf{D}_s^i \mathbf{T} = \begin{bmatrix} \mathbf{L}_s \\ \mathbf{M}_s \end{bmatrix} \mathbf{T}$$

- (c) Calculate the cost function $J = \|\mathbf{H}_s^i \beta_s^i - \mathbf{T}\|^2 + C \|\beta_s^i\|^2$.
3. Choose the hidden node k that has the smallest cost function then: $\mathbf{H}_s = \mathbf{H}_s^k, \mathbf{D}_s = \mathbf{D}_s^k$ and $\beta_s = \beta_s^k$.
4. Calculate the new learning accuracy ϵ_s .

3 Application in Supervised Learning

In this section, we apply ELM and its variants to three supervised learning tasks. In the subsequent applications, a normal distribution with zero mean is adopted as the sampling distribution of the hidden nodes. The standard deviation, commonly referred to as the scale parameter in this context, is treated as an undetermined hyperparameter requiring empirical specification.

3.1 Learning Parametric Pricing Functions

We employ ELM to approximate the IVS function under the Heston and rough Heston stochastic volatility models. The framework processes inputs (Θ, T, k) , where Θ denotes the set of model parameters, T represents the option's time to maturity, and $k \equiv \frac{K}{F_0}$ represents moneyness (where K is the strike price and F_0 denotes the current forward price). Learning parametric pricing functions via DNN are constrained by the model parameter bounds defined during the training phase. In other words, the model parameters—such as those used in option pricing—are confined to predefined lower and upper bounds. If market data falls outside this range (e.g., time to maturity exceeds the trained upper limit defined during the training dataset), the DNN may require retraining to accommodate the new values. In contrast, ELMs offer an efficient alternative that facilitates rapid adaptation to expanded parameter domains without suffering from slow retraining.

We generate implied volatility from numerical solutions using the COS method, which yields a dataset of 100,000 samples. Each input vector comprises seven (eight) dimensions: $(k, T, \rho, \kappa, \sigma, \theta, v_0)$ for Heston ($(k, T, \rho, \alpha, \gamma, \nu, \theta, v_0)$ for rough Heston), where k spans $[0.714, 1.667]$ for Heston and $[0.6, 1.4]$ for rough Heston, and T ranges from 0.10 to 3.00 years for Heston and from 0.05 to 3.00 years for rough Heston. Consider a risk-neutral filtered probability space $(\mathbb{Q}, \Omega, \mathcal{F}, \{\mathcal{F}_t\}_{t \geq 0})$, $(\rho, \kappa, \sigma, \theta, v_0)$ correspond to Heston model parameters governing correlation, mean reversion rate, volatility of volatility, long-term variance, and initial variance, respectively:

$$\begin{cases} dS_t/S_t = rdt + \sqrt{v_t}dW_t \\ dv_t = \kappa(\theta - v_t)dt + \sigma\sqrt{v_t}dZ_t, \end{cases}$$

where $dW_t dZ_t = \rho dt$ with \mathbb{Q} -Brownian motions W and Z . Furthermore, $\rho, \alpha, \gamma, \nu, \theta, v_0$ correspond to rough Heston model parameters that govern correlation, roughness, mean reversion rate, volatility of volatility, long-term variance, and initial variance, respectively:

$$\begin{cases} dS_t/S_t = rdt + \sqrt{v_t}dW_t, \\ v_t = v_0 + \frac{1}{\Gamma(\alpha)} \int_0^t (t-s)^{\alpha-1} \gamma (\theta - v_s) ds + \frac{1}{\Gamma(\alpha)} \int_0^t (t-s)^{\alpha-1} \gamma \nu \sqrt{v_s} dZ_s, \end{cases} \quad (4)$$

where $dW_t dZ_t = \rho dt$ as before.

The parameter ranges of Heston model are $\rho \in (-1, 0), \kappa \in (0, 4), \sigma \in (0, 0.5), \theta \in (0, 0.1), v_0 \in (0, 0.5)$, and those of rough Heston model are $\rho \in (-0.9, 0), \alpha \in (0.55, 0.95), \gamma \in (0.01, 3.0), \nu \in (0.01, 1.0), \theta \in (0.15, 0.5), v_0 \in (0.5, 1.0)$. The output implied volatility values exhibit a mean of 0.276 (0.230) and a standard deviation of 0.177 (0.141) for the Heston (rough Heston) model. The dataset is partitioned into two subsets: 80,000 training samples and 20,000 test samples.

We first examine the dependence of the ELM performance on the network sampling distribution's scale parameter and the hidden node number. Figure 1 demonstrates

these relationships: the left panel illustrates RMSE variation in the test sample with respect to the distribution scale, while the right panel quantifies test-sample RMSE as a function of node number. The error converges as neurons increase. The scale parameter selection, however, reveals an inherent trade-off. Excessively small scale values make the network too restrictive by limiting the diversity of features generated through weight and bias configurations. Conversely, excessively large scale parameters induce sparsity in the feature representations produced during training, which requires a larger node number to maintain approximation accuracy. An well-learned pricing function therefore requires balancing the node number with scale parameters.

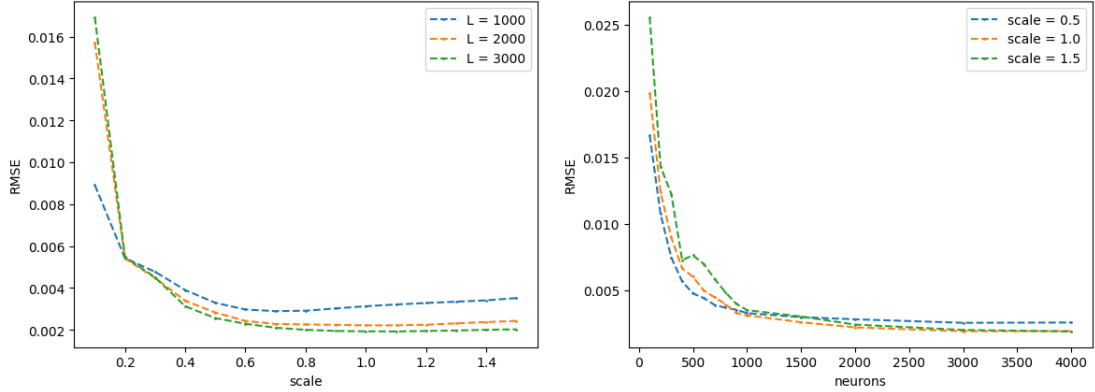


Figure 1: Performance under different network parameters on the testing dataset. The left subfigure illustrates the variation in RMSE across the dataset with respect to the scale parameter of the sampling distribution, while the right subfigure demonstrates the relationship between RMSE and the number of hidden nodes in the network. A sine activation function is employed throughout the analysis, with all experiments conducted using a sample size of 100,000.

To empirically demonstrate ELM’s comparative advantages, we compare the small-sample (under size 20,000) performance of ELM with GPR method. A brief introduction of GPR can be found in Appendix B. The GPR implementation aligns with the specifications outlined in [De Spiegeleer et al. \(2018\)](#).

We first compare the training process between ELM and GPR. As evidenced in Table 1, an ELM architecture with 3,000 hidden nodes achieves predictive accuracy comparable to GPR while training several times faster. While GPR has much smaller training error, it requires constructing an $N \times N$ kernel matrix that results in a computational complexity scaling fast with data size. In comparison, ELM’s computational complexity mainly scales with the neuron number under the Cholesky decomposition. Figure 2 further elucidates this disparity through the comparison of training time and testing RMSE of Heston model (first row) and rough Heston model (second row): the right column confirms at least comparable performance metrics, while the left column shows

Table 1: Comparison of ELM and GPR performance on Heston and rough Heston models. ELM configurations with 1000 and 3000 hidden nodes are shown. A sine activation is employed for ELM. Both GPR and ELM are performed without tuning hyperparameters. The sample is randomly selected from the original data with size 15,000 for both models. Indicator MAE stands for mean absolute error and indicator MAPE stands for mean absolute percentage error calculated as $|(y_{\text{pred}} - y_{\text{true}})/y_{\text{true}}| \times 100\%$.

	CPU Time (s)	RMSE	MAE ¹	MAPE (%) ²
Panel A: Training Process				
Panel A.1: Heston Model				
ELM (1000)	0.48	0.00235	0.00163	3.98
ELM (3000)	2.23	0.00090	0.00062	1.54
GPR	14.71	9.66×10^{-6}	5.45×10^{-6}	0.13
Panel A.2: Rough Heston Model				
ELM (1000)	0.73	0.00177	0.00116	3.05
ELM (3000)	2.53	0.00077	0.00051	1.23
GPR	15.50	7.36×10^{-7}	4.11×10^{-7}	0.02
Panel B: Testing Process				
Panel B.1: Heston Model				
ELM (1000)	0.05	0.00292	0.00190	5.28
ELM (3000)	0.15	0.00173	0.00102	3.27
GPR	0.27	0.00243	0.00129	5.13
Panel B.2: Rough Heston Model				
ELM (1000)	0.06	0.00201	0.00130	4.32
ELM (3000)	0.15	0.00135	0.00080	2.96
GPR	0.26	0.00160	0.00060	1.58

that ELM’s computational time scales steadily and slowly with dataset size. In contrast, GPR exhibits rapid escalation in computational cost.

We then compare the inference speed between ELM, GPR and DNN. Deep neural networks are needed for the problems of deep calibration or deep option pricing. We intend to show the efficiency of a single-layer network like ELM in the inference procedure. To this end, a DNN with a commonly used four-layer structure, each with 750 neurons, is incorporated. Note that the total number of neurons in DNN is the same in ELM. Figure 3 evaluates the CPU time requirements of inference in varying batch sizes, where the test sample is divided into batches of specified size, and the testing time represents the cumulative execution duration across all batches. Experimental results indicate that, with comparable testing performances, ELM achieves superior computational speed compared to GPR and DNN. Under optimized batch sizes, ELM can infer several times faster than GPR.

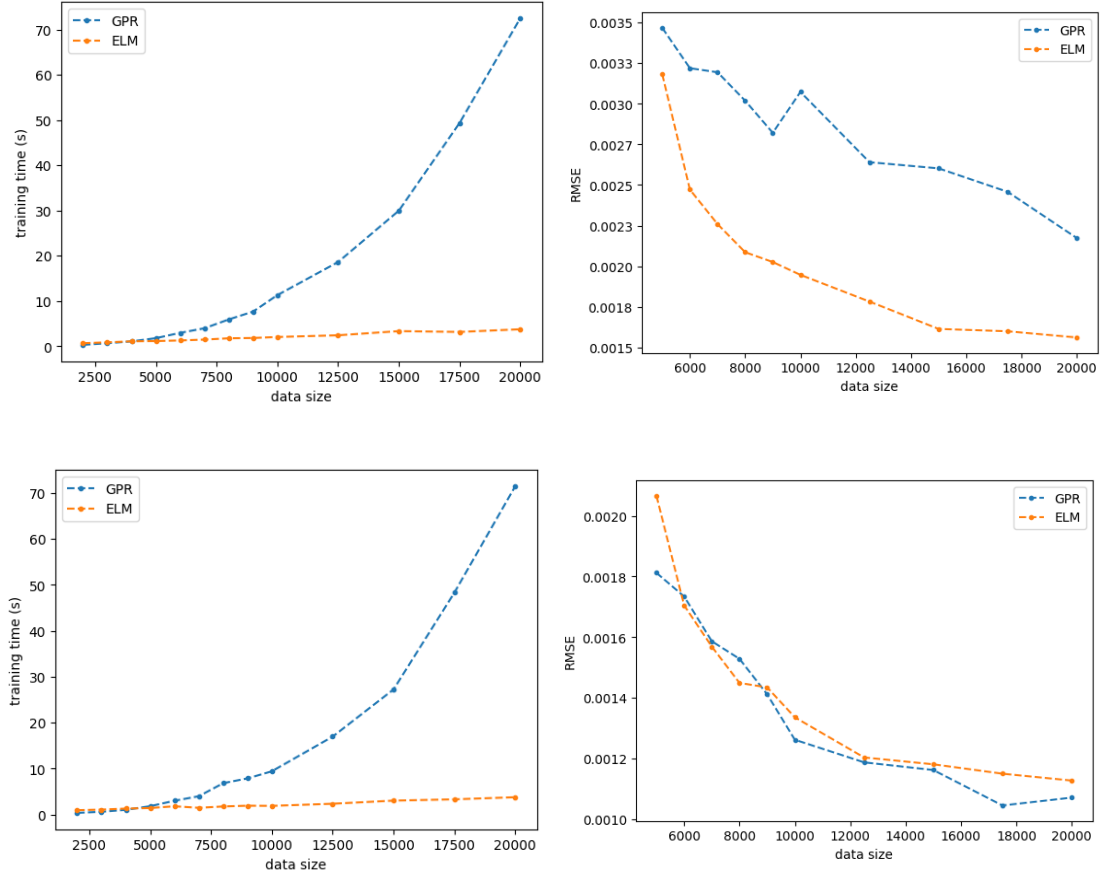


Figure 2: Comparison of training speed between ELM ($L = 3000$) and GPR in the tasks of learning Heston pricing model (first row) and rough Heston pricing model (second row). Both GPR and ELM are performed without tuning hyper-parameters. The left panel shows the increase in training time with respect to data size, and the right panel shows the corresponding out-of-sample RMSE in a testing sample size 3000.

As also shown in Figure 3, the batch size of ELM/DNN can be significantly larger than that of GPR. This is because the dimensionality of the kernel matrix of GPR grows linearly with data size, leading to a computational complexity of $O(N^3)$ and spatial complexity $O(N^2)$, making it impractical for large datasets ($N > 10^5$). ELM circumvents this constraint through fixed-dimensional computations governed by the hidden node number (e.g. Cholesky decomposition with $O(L^3)$ computational complexity and spatial complexity increasing linearly with data size), which ensures both training efficiency and low memory requirements to large-scale tasks.

In summary, we find that with learning accuracy resembling GPR, ELM can train as

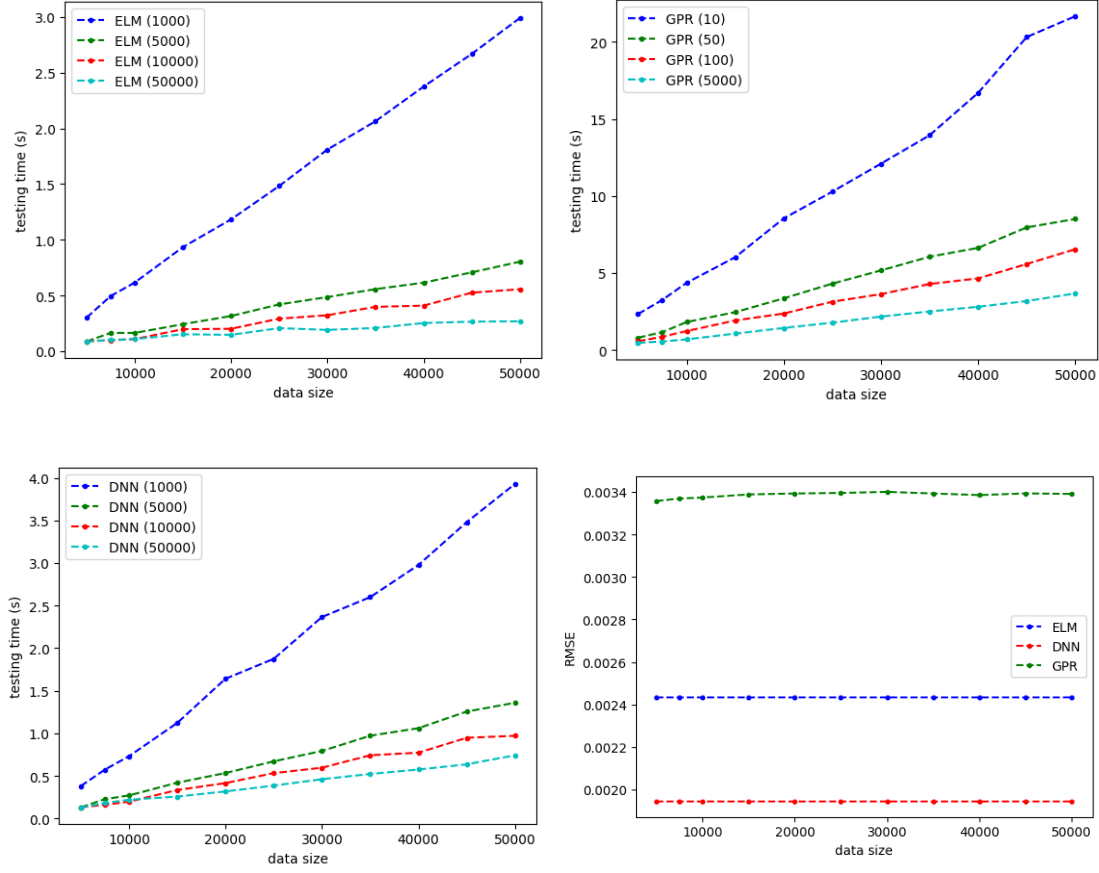


Figure 3: Comparison of the inference speed between ELM ($L = 3000$), GPR and DNN (four hidden layers with $L = 750$ in each layer). A training sample of 12,000 is used. And the testing procedure is performed on a 3000 sample size under different batch sizes in order to avoid the memory issue

well as infer much faster. In particular, the inference speed is important in practice, and ELM can be applied to large-scale datasets with better efficiency and memory requirements. In addition, a multi-layer DNN with the same number of neurons infer slower than ELM, making ELM a possible alternative for the deep calibration problem. Finally, we also examine how the EIR-ELM streamlines network architecture through strategic node selection, see Appendix C for details.

3.2 Return Prediction

This study implements ELM and LR to forecast directional movements in intraday stock prices. The dataset comprises high-frequency price data and order book records for Ping

An Bank (000001.XSHE) from January 2, 2020 to December 31, 2022. We define the binary target variable $y(i)$ as:

$$y(i) = \begin{cases} +1 & \text{if } S_{t_i+\Delta t} \geq S_{t_i} \\ -1 & \text{otherwise,} \end{cases}$$

where $\Delta t = 5$ minutes, and S_t denotes the asset price at time t . This encodes the direction of 5-minute price changes for binary classification. Twelve predictive features, derived from tick-level transaction histories and limit order book dynamics (detailed in Appendix A), constitute the input vector.

Of the twelve quarters in the dataset, we consecutively select eight quarters for the evaluation of ELM and LR, with a total of three consecutive periods: 2020-01-02 \sim 2021-12-31, 2020-07-01 \sim 2022-06-30, 2021-01-04 \sim 2022-12-30. For each window, models are initially trained on the first six quarters. During the subsequent two-quarter testing phase, daily recalibration is performed by incrementally integrating the prior trading day’s data, ensuring continuous adaptation to evolving market conditions.

Table 2: Performance comparison between ELM and LR models. For each training/test set, the first value represents classification accuracy (%) and the second value shows the F1-score (%). Compared with classification accuracy, F1-score takes into account the imbalance in the class distribution.

ELM configurations used 30/300 hidden nodes with sine activation and simulation scale = 0.01. LR was trained for 1000 iterations to ensure convergence.

	Training		Test		CPU Time (s)
	Accuracy	F1-score	Accuracy	F1-score	
Period 1					
ELM (30)	55.69	47.98	54.65	45.92	1.77
ELM (300)	54.98	53.02	53.47	50.42	24.98
LR	55.53	45.60	54.98	43.60	42.15
Period 2					
ELM (30)	55.18	47.15	56.38	42.76	1.80
ELM (300)	54.23	52.57	52.95	49.54	20.81
LR	55.02	44.95	56.46	41.78	41.65
Period 3					
ELM (30)	56.19	48.22	59.06	44.63	1.78
ELM (300)	54.66	53.06	56.16	52.58	30.19
LR	55.79	45.48	59.00	44.13	42.03
Whole Period					
ELM (30)	56.08	47.41	58.61	44.94	4.05
ELM (300)	55.32	52.64	57.14	51.76	41.48
LR	55.92	45.27	58.48	43.86	88.89

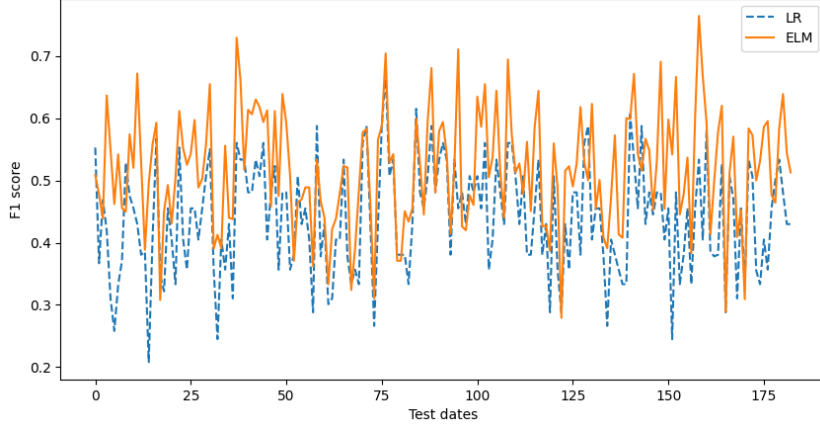


Figure 4: Out-of-sample classification F1 score of ELM ($L = 300$) and LR. The test period is from 2022-04-01 to 2022-12-31.

LR is a fundamental supervised learning algorithm used primarily for binary classification tasks, where the goal is to predict one of two possible outcomes. Unlike linear regression, which predicts continuous values, logistic regression predicts probabilities using the logistic function, mapping outputs to a range between 0 and 1.

Table 2 compares the predictive capabilities of ELM and LR under fixed architectural parameters ($L = 30$ hidden nodes, scale parameter = 0.01). The results demonstrate ELM’s superior training accuracy relative to LR, while maintaining at least equivalent out-of-sample performance. This sustained advantage is further corroborated by Figure 4, which visualizes daily classification accuracy throughout the test period. From the figure, ELM achieves better classification accuracy in average, while requiring significantly less computational time for model training.

The results can be justified by the network structure of ELM, which generates more complicated interactions between variables. In addition, LR requires iterative algorithms to converge to a solution while ELM directly estimates its network parameters, which makes ELM much faster for small neuron numbers.

3.3 Completing IVS

This experiment evaluates ELM for reconstructing implied volatility surfaces (IVS) using S&P 500 options data sourced from OptionMetrics (January 4 – February 28, 2023). Specifically, we learn the mapping from option moneyness and maturity to the corresponding implied volatility. To train the mapping, we follow the following procedure:

1. For each time to maturity, we obtain the risk-free rate from interpolating the treasury bill rates on the given date.
2. Obtain option log moneyness from $k \equiv \frac{K}{F_t} = \frac{K}{S_t} e^{rT}$.
3. Learn the mapping $(T, k) \mapsto IV$ by an ELM/GPR framework.

To reduce the data noise, we clean the data according to the following criteria (following the standard procedure in [Bardgett et al. \(2019\)](#)). We remove observations that

- are in-the-money ($k > 0$ for put options and $k < 0$ for call options)
- violate of standard arbitrage conditions
- have log moneyness outside $[-1.2, 0.3]$
- exceed 3.0 years to maturity
- have missing implied volatility values

After cleaning, the dataset contains an average of 2,658 daily implied volatility points, whose distributions are displayed in Appendix D. We then partition the dataset into 80% training and 20% testing subsets via random sampling.

For benchmark comparison, GPR is implemented under the design that aligns with [De Spiegeleer et al. \(2018\)](#) with kernel parameters optimized through grid-based searching. The ELM configuration utilizes a hyperbolic tangent activation function, 1,000 hidden nodes ($L = 1000$), and a fixed scale parameter $\sigma = 0.5$. We highlight the methodological difference that no parameter is tuned in ELM during the training process.

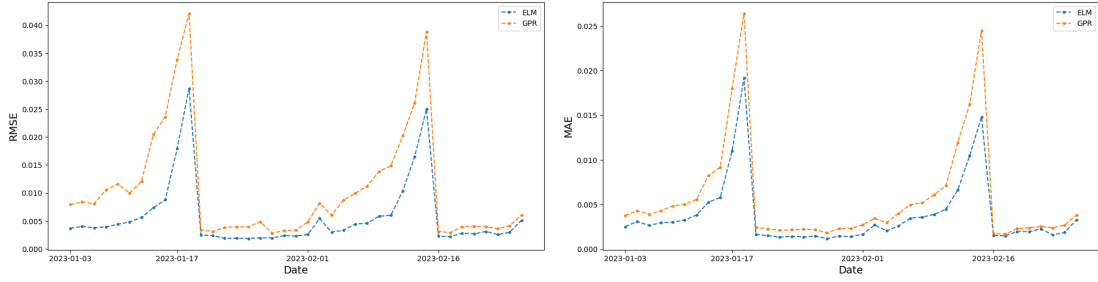


Figure 5: The RMSE (left) and MAE (right) of ELM and GPR in the test sample. The ELM uses a hyperbolic tangent activation function with $L = 1000$ and $\sigma = 0.5$. The GPR configuration aligns with [De Spiegeleer et al. \(2018\)](#) with kernel parameters optimized through grid-based searching.

Figure 5 compares the out-of-sample predictive accuracy of ELM and GPR in implied volatility surface completion. Despite operating without hyperparameter optimization, ELM systematically outperforms GPR across all testing dates throughout the evaluation period.

After completing the IVS for each date, we validate the non-arbitrage condition of the trained model through the following numerical procedure.

Step 1 Create a meshgrid of $\{(T_i, K) \mid i = 1, \dots, N\}$ based on the boundaries of the original input data.

Step 2 Compute model IVS by applying the pre-trained ELM on the meshgrid.

Step 3 Assume the current price of the underlying $S = 1$, compute the call prices by applying the Black-Scholes formula.

Step 4 Validate the absence of arbitrage by checking the following conditions for $C(K, T)$ defined on $K \in [\min K_i, \max K_i]$ and $T \in [\min T_i, \max T_i]$ (Roper (2010)):

1. $C(K, \cdot)$ is non-decreasing for $K \in [\min K_i, \max K_i]$.
2. $C(\cdot, T)$ is non-increasing for $T \in [\min T_i, \max T_i]$.
3. $C(\cdot, T)$ is a convex function for $T \in [\min T_i, \max T_i]$.

We examine the non-arbitrage conditions on the IVS of range $K \equiv e^k \in [0.7, 1.2]$ and $T \in [0.05, 1]$. The IVS range is discretized evenly into a meshgrid 100×100 . We define the violation rate of arbitrage of type one as the percentage of moneynesses under which $C(K, \cdot)$ is not non-decreasing. The violation rates of the other two types are defined likewise.

The numerical tests in Figure 6 show that both methods admit no arbitrage opportunities on most dates of the two-month period, but admit some arbitrage of the three types on certain dates that correspond to the relatively high out-of-sample error test shown in Figure 5. In general, ELM-generated IVS admits fewer violations than GPR, more prominently in terms of the convexity condition.

The disparity likely stems from fundamental methodological differences: GPR’s propensity to overfit localized noise patterns amplifies surface irregularities, whereas ELM’s generalization capacity – controlled through architectural parameters (node number and scale parameter) – enforces smoother representations. In fact, Jacot et al. (2018) argues that the kernel in GPR acts similarly to the dynamics of an ANN in the infinite-width limit, which makes the training and generalization properties of wide ANNs analogous to those of GPR. Compared to ELM, whose structure is equivalent to a single-layer ANN, the interpolation capability of a multilayer equivalence is more likely to overfit. Figure 7 explores the disparity by comparing the monotonicity and convexity of $C(K, T)$ directly in both methods. We see from the left subplot that the ELM-generated IVS tends to be more robust with smoother temporal derivatives. In addition, the bumps generated by GPR observed in $d^2C(K)$ are absent in ELM-generated IVS, which also demonstrates the superior IVS-completing performance of ELM.

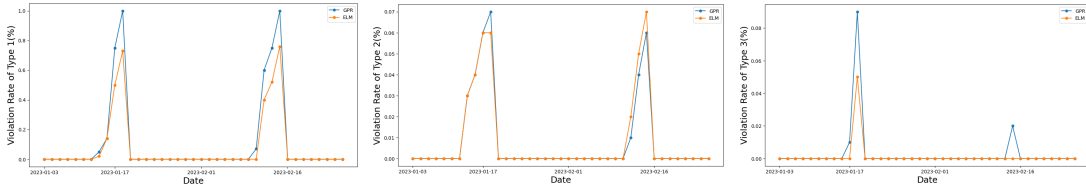


Figure 6: Violation rates of the monotonicity condition of T (left), K (middle) and the convexity condition (right) in ELM and GPR method. The violation rate is defined as the percentage of moneynesses (maturities) where the non-decreasing (convexity) condition is not satisfied.

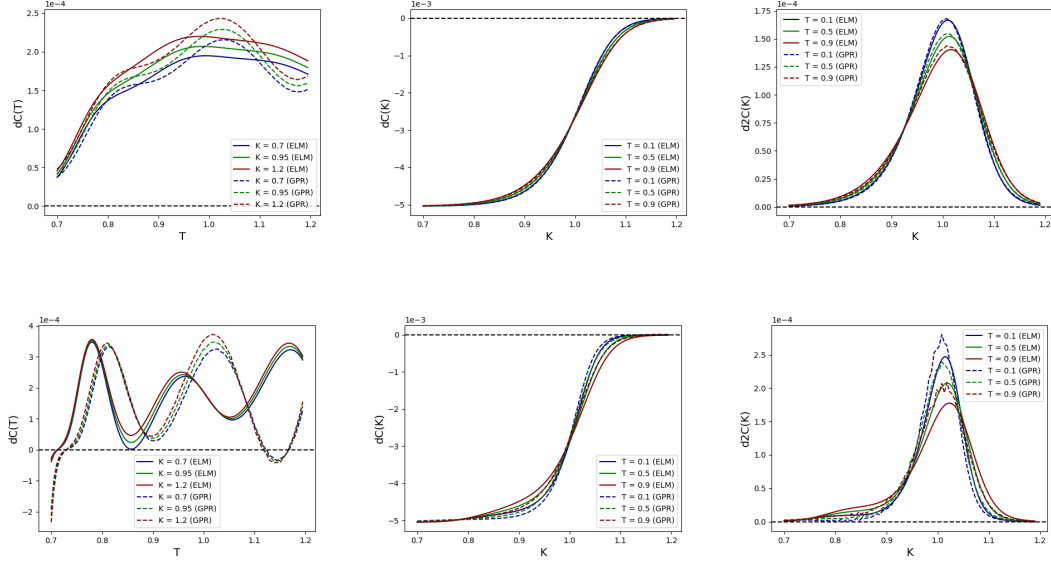


Figure 7: Validation of the non-arbitrage conditions on 2023-01-03 (first row, no arbitrage observed) and on 2023-01-18 (second row, arbitrage observed). The x-axis is discretized into 100 points and the values represent the first-order difference $dC(T)$, $dC(K)$, and the second-order difference $d^2C(K)$.

4 Application in Unsupervised Learning

In this section, we apply ELM to solve the PDE systems that characterize the prices of exotic options. We will first introduce the theory of Physics informed ELM. Then we conduct specific experiments in derivative products including European options, rainbow options, and barrier options.

Compared with other numerical methods such as finite difference, finite element or DNN (e.g. Physics informed neural network) method, ELM solves more rapidly since it formulates a linear PDE into a linear equation system and solve the equations using efficient matrix decomposition methods. In fact, it was shown in [Dwivedi and Srinivasan \(2020\)](#) that it takes ELM a few seconds to solve a linear PDE where DNN takes hours to achieve a comparable accuracy. We also note that ELM shows promising ability in high-dimension problems, which is further elaborated in [Gonon \(2023\)](#).

Consider the following PDE system:

$$\begin{cases} \frac{\partial}{\partial t} u(\vec{x}, t) + \mathcal{L}u(\vec{x}, t) = R(\vec{x}, t), & (\vec{x}, t) \in \Omega \times [0, T] \\ u(\vec{x}, t) = B(\vec{x}, t), & (\vec{x}, t) \in \partial\Omega \times [0, T], \\ u(\vec{x}, 0) = F(\vec{x}), & \vec{x} \in \Omega, \end{cases}$$

where \mathcal{L} is a linear differential operator and $\partial\Omega$ is the boundary of computational domain Ω . Dwivedi and Srinivasan (2020) proposed a Physics informed ELM to approximate $u(\mathbf{x}, t)$ by the output of ELM: $u(\vec{x}, t) = \text{ELM}(\mathbf{x}, t)$. Suppose that $\Omega \in \mathbf{R}^d$. Define $\mathbf{X} = [\mathbf{x}, t, 1]^\top$, $\mathbf{w}^X = [\mathbf{w}_1^X, \mathbf{w}_2^X, \dots, \mathbf{w}_L^X]^\top$, $\mathbf{w}^T = [w_1^T, w_2^T, \dots, w_L^T]^\top$ and $\mathbf{b} = [b_1, b_2, \dots, b_L]$. Under the weights and bias of the hidden layer given by $(\mathbf{w}^X, \mathbf{w}^T, \mathbf{b})$, the output of the k -th hidden neuron is then

$$h_k = G(z_k) \quad k = 1, 2, \dots, L$$

for activation function $G(\cdot)$, where $z_k = [\mathbf{w}_k^X, w_k^T, b_k] \cdot \mathbf{X}$. The ELM output is given by

$$f(\mathbf{X}) = \mathbf{h}_{1 \times k} \boldsymbol{\beta}_{k \times 1}.$$

We can derive from the operations in the ELM network that

$$\begin{cases} \frac{\partial^p f_k}{\partial x_l^p} = (w_{kl}^X)^p \frac{\partial^p G}{\partial \mathbf{z}^p} \boldsymbol{\beta}, \quad p = 1, 2 \\ \frac{\partial f_k}{\partial t} = w_k^T \frac{\partial G}{\partial \mathbf{z}} \boldsymbol{\beta}, \end{cases}$$

where $l = 1, 2, \dots, d$ and $k = 1, 2, \dots, L$. The mixed partial derivatives can be deduced likewise.

In the training process, we randomly sample points (\mathbf{x}, t) with number N_f, N_{bc}, N_{ic} in the domain $\Omega \times [0, T]$, boundary $\partial\Omega \times [0, T]$ and $\Omega \times T$, respectively. We define the corresponding training errors as $\boldsymbol{\xi}_f$, $\boldsymbol{\xi}_{bc}$ and $\boldsymbol{\xi}_{ic}$ with

$$\begin{cases} \boldsymbol{\xi}_f = \frac{\partial f}{\partial t} + \mathcal{L}f - R, & (\mathbf{x}, t) \in \Omega \times [0, T], \\ \boldsymbol{\xi}_{bc} = f - B, & (\mathbf{x}, t) \in \partial\Omega \times [0, T], \\ \boldsymbol{\xi}_{ic} = f(\cdot, 0) - F, & \mathbf{x} \in \Omega. \end{cases}$$

To solve the linear PDE, we need to minimize $\|\boldsymbol{\xi}_f\|_2^2 + \|\boldsymbol{\xi}_{bc}\|_2^2 + \|\boldsymbol{\xi}_{ic}\|_2^2$, which leads to a linear equation system represented as

$$\mathbf{H} \cdot \boldsymbol{\beta} = \mathbf{Y},$$

where $\mathbf{H} \in \mathbf{R}^{N \times L}$, with $N = N_f + N_{bc} + N_{ic}$, is the hidden matrix determined by the linear operator and the network configuration, and \mathbf{Y} depends on functions R , B and F given by the PDE. We generally set $N > L$ to ensure a sufficiently large training set.

Finally, the solution of the linear equation system under least squared error is given by Moore–Penrose generalized inverse: $\boldsymbol{\beta} = (\mathbf{H}^\top \mathbf{H} + C\mathbf{I})^{-1} \mathbf{H}^\top \mathbf{Y}$, which is equivalent to the solution of the following optimization problem: $\arg \min_{\boldsymbol{\beta}} J$, where

$$J = \frac{1}{2} C \|\boldsymbol{\beta}\|^2 + \frac{1}{2} \left(\frac{\boldsymbol{\xi}_f^\top \boldsymbol{\xi}_f}{N_f} + \frac{\boldsymbol{\xi}_{bc}^\top \boldsymbol{\xi}_{bc}}{N_{bc}} + \frac{\boldsymbol{\xi}_{ic}^\top \boldsymbol{\xi}_{ic}}{N_{ic}} \right),$$

with the regularization parameter C . Increasing C can enhance the generalization ability of ELM.

Next, we apply the theory of physics informed ELM to solve the price of exotic options whose terminal condition, instead of initial condition, is known. The call price of a European option is

$$V(t, \mathbf{u}) = e^{-r(T-t)} \mathbb{E}[H(\mathbf{S}_T) \mid \mathbf{S}_t = e^{\mathbf{u}}],$$

which is the unique viscosity solution of the partial differential equation

$$\frac{\partial V}{\partial t}(t, \mathbf{u}) + \frac{1}{2} \sum_{1 \leq i, j \leq m} \rho_{ij} \sigma_i \sigma_j \frac{\partial^2 V}{\partial u_i \partial u_j}(t, \mathbf{u}) + r \sum_{l=1}^m \frac{\partial V}{\partial u_l}(t, \mathbf{u}) - rV(t, \mathbf{u}) = 0, \quad (t, \mathbf{u}) \in (0, T) \times \mathbb{R}^m,$$

with terminal condition $V(T, \mathbf{u}) = H(\mathbf{u})$ and $u_l = \ln S_l$, $l = 1, \dots, m$.

When $m = 1$ and $H(u) = (K - e^u)^+$, the put option admits the analytic price

$$V(t, u) = e^u \mathcal{N}(d_1) - K e^{-r(T-t)} \mathcal{N}(d_2),$$

where

$$d_2 = \frac{1}{\sigma \sqrt{T}} \left(u - \ln(K) + \left(r - \frac{\sigma^2}{2} \right) T \right)$$

and $d_1 = d_2 + \sigma \sqrt{T}$.

We further define the relative error as

$$\text{RE} = \frac{\|V_{\text{True}} - V_{\text{ELM}}\|_2}{\|V_{\text{True}}\|_2}.$$

Figure 8 shows the performance of ELM in put options for $m = 1$. The relative error is 0.00059 for $\sigma = 0.25$ and 0.00143 for $\sigma = 0.5$. We also calculate on the implied volatility surface ($T \in [0, 1)$, $S \in [0, 60]$) a mean relative error of 0.00076 for $\sigma = 0.25$ and 0.00103 for $\sigma = 0.5$.

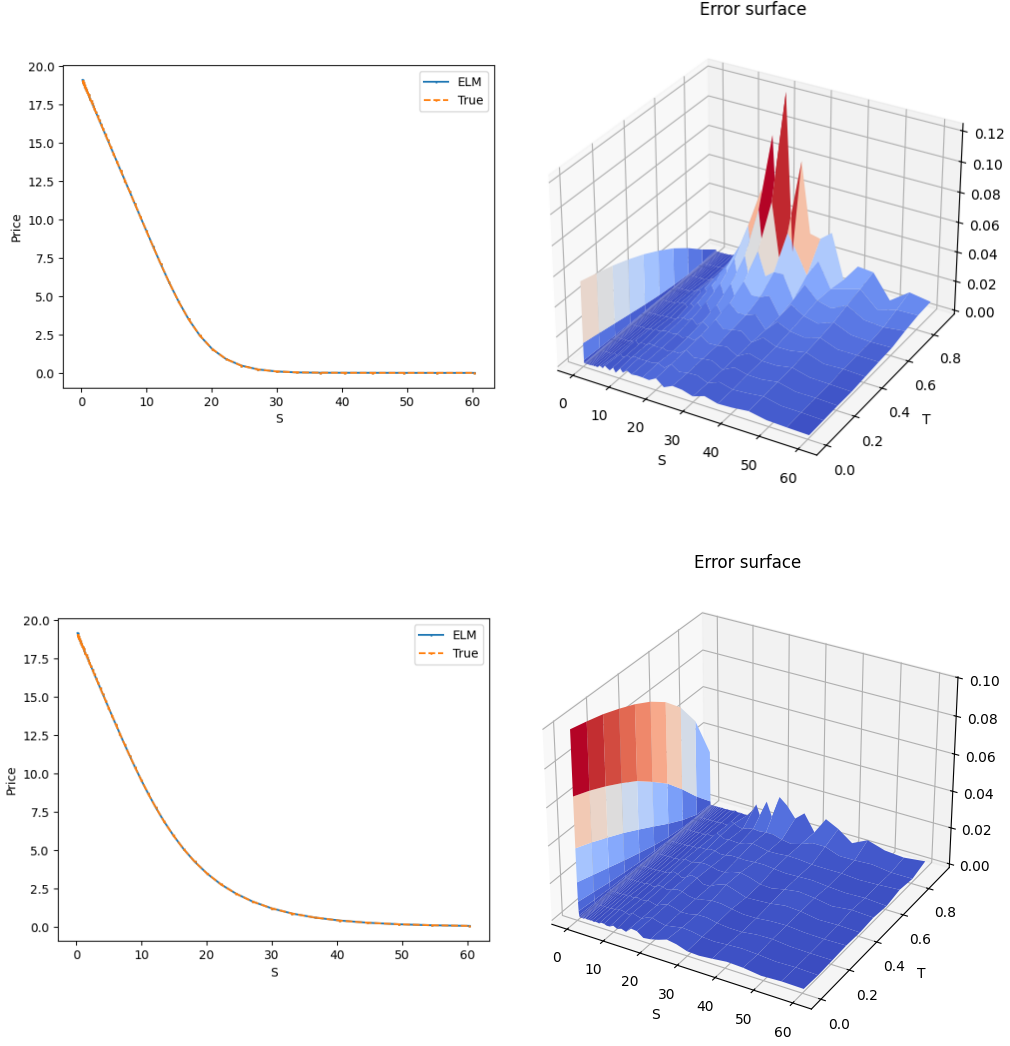


Figure 8: Comparison of ELM predictions and the analytical prices for put options. We set $r = 0.04$, $T = 1$ with hidden node number 5000 and scale 1. The hyperbolic tangent function, as chosen in [Dwivedi and Srinivasan \(2020\)](#), is adopted as the activation function. The left column compares the predictions and the Black-Scholes prices under $K = 15$, with the relative errors 0.00059 ($\sigma = 0.25$, first row) and 0.00143 ($\sigma = 0.5$, second row). And the right column shows the L^1 option price errors across different maturities and initial prices, with mean relative errors 0.00076 (first row) and 0.00103 (second row).

As an example of dimension $m = 2$, given $H(\ln \mathbf{S}_T) = \max\{K - \max\{S_{1,T}, S_{2,T}\}, 0\}$, the payoff of a put rainbow option on maximum of two assets, we examine how ELM produces the price of a rainbow option. The analytical price formula of rainbow options

can be found in [Stulz \(1982\)](#). Figure 9 shows that the relative error at $T = 1$ is 0.00294 for $\rho = 0$ and 0.00545 for $\rho = -0.95$. The performance is weaker than the 1-dimensional European options, but is still good enough in practice.

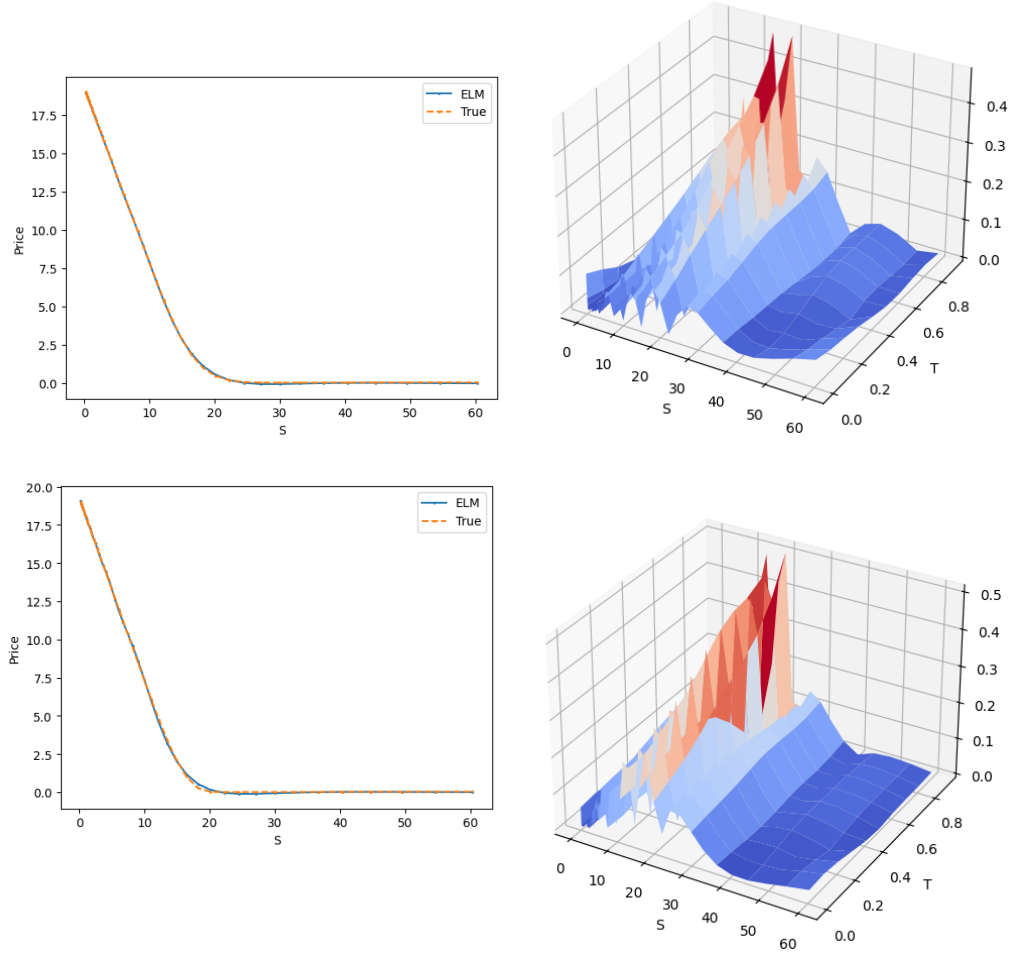


Figure 9: Comparison of ELM predictions and the analytical prices for rainbow put options. We set $r = 0.04$, $\sigma = 0.25$, $T = 1$ with hidden node number 5000 and scale 1. The left column compares the predictions and the Black-Scholes prices under $K = 20$, with the relative errors 0.00294 for $\rho = 0$ (first row) and 0.00545 for $\rho = -0.95$ (second row). And the right column shows the L^1 option price errors across different maturities and initial prices, with mean relative errors 0.00616 for $\rho = 0$ and 0.00776 for $\rho = -0.95$.

We also explore the application of ELM in barrier options. We consider a double-barrier call option whose price satisfies the following PDE system:

$$\begin{cases} \frac{\partial V}{\partial t}(t, u) + \frac{\sigma^2}{2} \sum_{l=1}^m \frac{\partial^2 V}{\partial u_l^2}(t, u) + r \sum_{l=1}^m \frac{\partial V}{\partial u_l}(t, u) - rV(t, u) = 0, & (t, u) \in (0, T) \times [L, U] \\ V(t, L) = 0, V(t, U) = 0, t \in [0, T] \\ V(T, u) = (e^u - K)^+, u \in (L, U). \end{cases} \quad (5)$$

where L, U are the knock-out bounds for the log price. Double-barrier options also admit analytic prices, as shown in Appendix E.

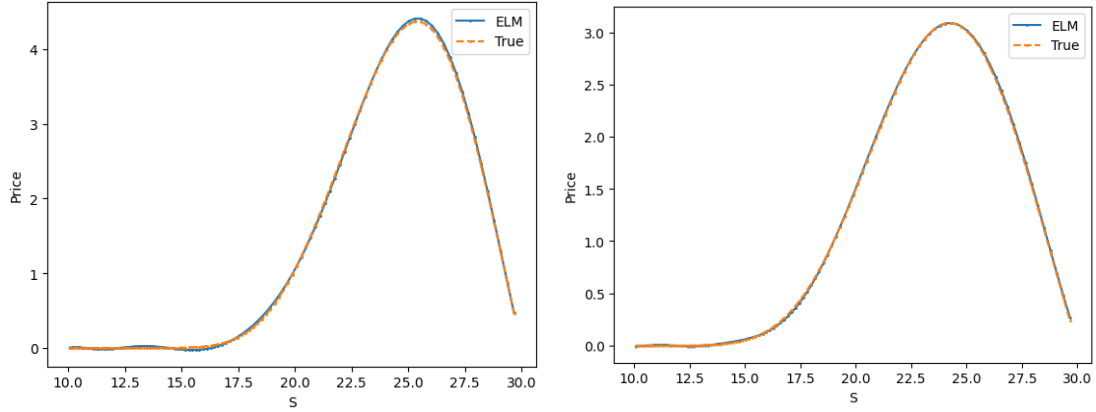


Figure 10: Comparison of ELM predictions and the analytical prices for knock-out double-barrier call options with lower and upper bound 10 and 30, respectively. We set $r = 0.04$, $\sigma = 0.15$, $K = 20$ with hidden node number 5000 and scale 1. The left (right) plot compares the predictions and the Black-Scholes prices under $T = 0.5$ ($T = 1$), with relative error 0.01343 (0.00909).

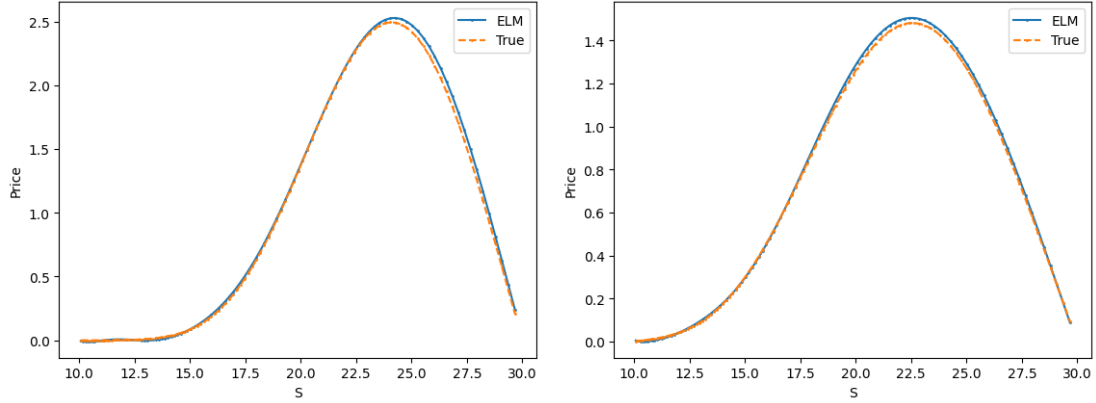


Figure 11: Comparison of ELM solutions and the analytical prices for knock-out double-barrier call options with lower and upper bound 10 and 30, respectively. We set $r = 0.04$, $\sigma = 0.25$, $K = 20$ with hidden node number 5000 and scale 1. The left (right) plot compares the predictions and the Black-Scholes prices under $T = 0.5$ ($T = 1$), with relative error 0.02489 (0.01831).

As $\tau \rightarrow 0$, the price of the knock-out double-barrier call option becomes volatile for S close to the upper bound. The option is more likely to be knocked out for large S , but also possibly pay off better for such initial prices. This sharp fall of the price around termination can result in greater discrepancy between ELM’s predictions and the true prices.

Remark 1 *Gonon (2023) demonstrates that ELM can overcome the curse of dimensionality and use the so-called true prices to demonstrate the approximation ability of ELM. We refer to Gonon (2023) for the corresponding analysis.*

5 Conclusions

This paper has investigated the application of extreme learning machines in quantitative finance, demonstrating their effectiveness across supervised and unsupervised learning. Our results establish ELM as a computationally efficient alternative to traditional methods with respect to training and inference procedures while maintaining competitive accuracy.

In supervised learning tasks, ELM excels in three critical scenarios. First, for learning pricing functions in stochastic volatility models, ELM achieves training speed orders of magnitude faster than DNNs and GPR. This efficiency advantage persists even when comparing the inference speed, with ELM several times faster while maintaining comparable pricing accuracy. In addition, the EIR-ELM variant is also shown to effectively

reduce model complexity without sacrificing accuracy in the task of learning pricing functions. Second, in high-frequency stock return forecasting, ELM classifiers outperform logistic regression in both accuracy and training speed ($20\times$ faster), which demonstrates its advantages for intraday trading data analysis. Third, for constructing implied volatility surfaces, ELM generates arbitrage-free surfaces with smoother derivatives and fewer arbitrage violations than GPR, making it more robust and practical in applications.

For unsupervised PDE solving, ELM overcomes key limitations of DNN-based approaches. In terms of training efficiency, ELM-based PINNs solve Black-Scholes-type equations orders-of-magnitude faster than traditional DNN implementations, which results from its formation of the problem as a linear equation system. Regarding high-dimensional PDEs, ELM is also shown to obtain promising accuracy.

Two promising future discussions emerge from this work. First, extending ELM-based PINNs to other path-dependent derivatives, such as American options and credit derivatives with early exercise features, remains an open challenge. Second, integrating ELM with online learning frameworks could enable real-time recalibration in non-stationary markets, further enhancing their practicality in trading and risk management.

In summary, this work positions ELM as a versatile tool for quantitative finance that combines the speed of traditional numerical methods with the flexibility of machine learning in supervised and unsupervised learning, which makes ELM potentially compelling for high-frequency trading systems, real-time risk management, and multi-asset derivative pricing.

References

- Chris Bardgett, Elise Gourier, and Markus Leippold. Inferring volatility dynamics and risk premia from the S&P 500 and VIX markets. *Journal of Financial Economics*, 131(3):593–618, 2019.
- Jan De Spiegeleer, Dilip B Madan, Sofie Reyners, and Wim Schoutens. Machine learning for quantitative finance: fast derivative pricing, hedging and fitting. *Quantitative Finance*, 18(10):1635–1643, 2018.
- Vikas Dwivedi and Balaji Srinivasan. Physics informed extreme learning machine (PIELM)—a rapid method for the numerical solution of partial differential equations. *Neurocomputing*, 391:96–118, 2020.
- Guorui Feng, Guang-Bin Huang, Qingping Lin, and Robert Gay. Error minimized extreme learning machine with growth of hidden nodes and incremental learning. *IEEE Transactions on Neural Networks*, 20(8):1352–1357, 2009.
- Lukas Gonon. Random feature neural networks learn Black-scholes type PDEs without curse of dimensionality. *Journal of Machine Learning Research*, 24(189):1–51, 2023.

- Jiequn Han, Arnulf Jentzen, and Weinan E. Solving high-dimensional partial differential equations using deep learning. *Proceedings of the National Academy of Sciences*, 115(34):8505–8510, 2018.
- Blanka Horvath, Aitor Muguruza, and Mehdi Tomas. Deep learning volatility: a deep neural network perspective on pricing and calibration in (rough) volatility models. *Quantitative Finance*, 21(1):11–27, 2021.
- Guang-Bin Huang and Lei Chen. Convex incremental extreme learning machine. *Neurocomputing*, 70(16-18):3056–3062, 2007.
- Guang-Bin Huang, Lei Chen, and Chee-Kheong Siew. Universal approximation using incremental constructive feedforward networks with random hidden nodes. *IEEE Transactions on Neural Networks*, 17(4):879–892, 2006a.
- Guang-Bin Huang, Qin-Yu Zhu, and Chee-Kheong Siew. Extreme learning machine: theory and applications. *Neurocomputing*, 70(1-3):489–501, 2006b.
- Côme Huré, Huy  n Pham, and Xavier Warin. Deep backward schemes for high-dimensional nonlinear PDEs. *Mathematics of Computation*, 89(324):1547–1579, 2020.
- Arthur Jacot, Franck Gabriel, and Cl  ment Hongler. Neural tangent kernel: Convergence and generalization in neural networks. *Advances in Neural Information Processing Systems*, 31, 2018.
- Antoine Jacquier and Zan Zuric. Random neural networks for rough volatility. *arXiv preprint arXiv:2305.01035*, 2023.
- Naoto Kunitomo and Masayuki Ikeda. Pricing options with curved boundaries. *Mathematical Finance*, 2(4):275–298, 1992.
- Shuaiqiang Liu, Anastasia Borovykh, Lech A Grzelak, and Cornelis W Oosterlee. A neural network-based framework for financial model calibration. *Journal of Mathematics in Industry*, 9(1):9, 2019.
- Ariel Neufeld and Philipp Schmock. Universal approximation property of Banach space-valued random feature models including random neural networks. *arXiv preprint arXiv:2312.08410*, 2023.
- Maziar Raissi, Paris Perdikaris, and George E Karniadakis. Physics-informed neural networks: A deep learning framework for solving forward and inverse problems involving nonlinear partial differential equations. *Journal of Computational physics*, 378:686–707, 2019.
- Michael Roper. Arbitrage free implied volatility surfaces. *preprint*, 2010.

- Johannes Ruf and Weiguan Wang. Neural networks for option pricing and hedging: a literature review. *Journal of Computational Finance*, 24(1):1–46, 2020.
- Justin Sirignano and Konstantinos Spiliopoulos. DGM: A deep learning algorithm for solving partial differential equations. *Journal of computational physics*, 375:1339–1364, 2018.
- RenéM Stulz. Options on the minimum or the maximum of two risky assets: analysis and applications. *Journal of Financial Economics*, 10(2):161–185, 1982.
- Jian Wang, Siyuan Lu, Shui-Hua Wang, and Yu-Dong Zhang. A review on extreme learning machine. *Multimedia Tools and Applications*, 81(29):41611–41660, 2022.
- Christopher Williams and Carl Rasmussen. Gaussian processes for regression. *Advances in neural information processing systems*, 8, 1995.
- Yu-chen Wu and Jun-wen Feng. Development and application of artificial neural network. *Wireless Personal Communications*, 102:1645–1656, 2018.
- Zhixin Xu, Min Yao, Zhaohui Wu, and Weihui Dai. Incremental regularized extreme learning machine and its enhancement. *Neurocomputing*, 174:134–142, 2016.

Appendix A Feature Descriptions

In the task of intraday stock price movement prediction, we construct 12 features features. We introduce the following notation to define the features:

- t_i : The timestamp of the beginning of the i -th interval in the baseline execution strategy.
- u_i : The timestamp of the i -th trade.
- P_i : The transaction price of the i -th trade.
- q_i : The transaction volume of the i -th trade.
- P_t : The stock price at time t , defined as the price of the most recent trade before or at time t :

$$P_t = P_{\max\{i: u_i \leq t\}}.$$

- $\mathcal{P}_{t,k}^{Bid}$: The set of the top k bid prices in the order book at time t .
- $\mathcal{P}_{t,k}^{Ask}$: The set of the top k ask prices in the order book at time t .
- $Q_{t,P}$: The volume of limit orders placed at price P in the order book at time t .
- $OI_{t,k}$: The order imbalance at the k -th level at time t , that is

$$OI_{t,k} = \frac{Q_{t,k}^{Bid} - Q_{t,k}^{Ask}}{Q_{t,k}^{Bid} + Q_{t,k}^{Ask}},$$

where

$$Q_{t,k}^{Bid} = \sum_{P \in \mathcal{P}_{t,k}^{Bid}} Q_{t,P}, \quad Q_{t,k}^{Ask} = \sum_{P \in \mathcal{P}_{t,k}^{Ask}} Q_{t,P}.$$

To predict the stock price at t_{i+1} , we consider two categories of features: features derived from historical transactions and features derived from the limit order book. In the following, we provide the framework for these features.

The features derived from historical transactions include:

- **Open Price:** The opening price of the time interval $[t_{i-1}, t_i)$. Open Price = $P_{t_{i-1}}$.
- **Close Price:** The closing price of the time interval $[t_{i-1}, t_i)$. Close Price = $\lim_{t \rightarrow t_i-0} P_t$.
- **High Price:** The highest price during the time interval $[t_{i-1}, t_i)$. High Price = $\max_{t \in [t_{i-1}, t_i)} P_t$.
- **Low Price:** The lowest price during the time interval $[t_{i-1}, t_i)$. Low Price = $\min_{t \in [t_{i-1}, t_i)} P_t$.
- **Volume-Weighted Average Price (VWAP):**

$$\text{VWAP} = \begin{cases} \frac{\sum_{u_i \in [t_{i-1}, t_i)} P_i q_i}{\sum_{u_i \in [t_{i-1}, t_i)} q_i}, & \sum_{u_i \in [t_{i-1}, t_i)} q_i > 0, \\ \text{Close Price}, & \text{otherwise.} \end{cases}$$

- **Time-Weighted Average Price (TWAP):**

$$\text{TWAP} = \frac{\int_{t_{i-1}}^{t_i} P_t dt}{t_i - t_{i-1}}.$$

- **Market Trading Volume:** The total market trading volume during the time interval $[t_{i-1}, t_i)$. Trade Volume = $\sum_{u_i \in [t_{i-1}, t_i)} q_i$.

The features derived from the limit order book include:

- **Order Imbalance at t_i :** The order imbalance for the top k buy and sell prices at time t_i . Order Imbalance $_{t_i,k}$ = $OI_{t_i,k}$, where $k = 1, 5, \infty$.
- **Time-Weighted Average Order Imbalance:** The time-weighted average order imbalance for the top k buy and sell prices over the past Δ period.

$$\text{TWA Order Imbalance}_{t_i,k}(\Delta) = \frac{\int_{t_i-\Delta}^{t_i} OI_{t,k} dt}{\Delta},$$

where $k = 1, 5, \infty$ and $\Delta = 5\text{min}$.

Appendix B A Brief Introduction of GPR

Gaussian Process Regression (GPR) is a non-parametric, Bayesian approach to regression that models a function $f(\mathbf{x})$ as a distribution over possible functions. It is fully defined by a mean function $m(\mathbf{x})$ and a covariance (kernel) function $k(\mathbf{x}, \mathbf{x}')$.

1. Prior Distribution:

$$f(\mathbf{x}) \sim \mathcal{GP}(m(\mathbf{x}), k(\mathbf{x}, \mathbf{x}')),$$

where $m(\mathbf{x})$ is often assumed zero for simplicity and $k(\mathbf{x}, \mathbf{x}')$ encodes similarity between inputs (e.g., RBF kernel).

2. RBF Kernel Example:

$$k(\mathbf{x}, \mathbf{x}') = \sigma_f^2 \exp\left(-\frac{\|\mathbf{x} - \mathbf{x}'\|^2}{2\ell^2}\right),$$

where σ_f^2 , ℓ are parameters representing signal variance and length scale, respectively.

3. Posterior Prediction: Given training data \mathbf{X} (inputs) and \mathbf{y} (outputs), the predictive distribution for a new input \mathbf{x}_* is Gaussian:

$$p(f_* | \mathbf{X}, \mathbf{y}, \mathbf{x}_*) = \mathcal{N}(\bar{f}_*, \mathbb{V}[f_*]),$$

from which we obtain the predictive mean:

$$\bar{f}_* = \mathbf{k}_*^T (\mathbf{K} + \sigma_n^2 \mathbf{I})^{-1} \mathbf{y}$$

and predictive Variance:

$$\mathbb{V}[f_*] = k(\mathbf{x}_*, \mathbf{x}_*) - \mathbf{k}_*^T (\mathbf{K} + \sigma_n^2 \mathbf{I})^{-1} \mathbf{k}_*,$$

where \mathbf{K} is the kernel matrix with the (i, j) term $K_{ij} = k(\mathbf{x}_i, \mathbf{x}_j)$, $\mathbf{k}_* := [k(\mathbf{x}_*, \mathbf{x}_1), \dots, k(\mathbf{x}_*, \mathbf{x}_N)]^T$, and σ_n^2 is the noise variance.

Appendix C Simplification of Network Structure Through EIR-ELM

In the task of learning the Heston pricing function, the EIR-ELM method attains GPR's performance (achieved via a 2,000-dimensional kernel matrix) using fewer than 350 nodes shown in Figure 12. Moreover, the network is further simplified as the selection degree k increases. This optimized configuration reduces memory overhead while maintaining computational efficiency during inference phases.

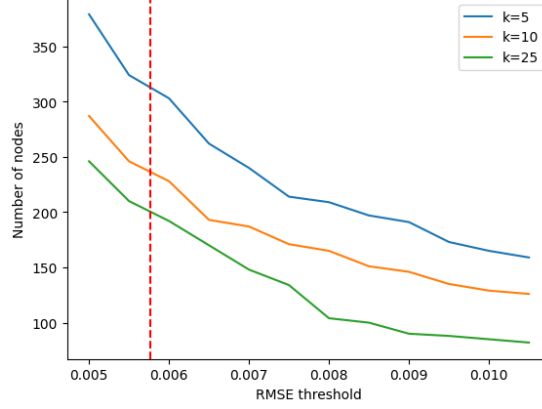


Figure 12: Simplification of neural network structure through EIR-ELM. The values correspond to the number of nodes needed to achieve the specified RMSE levels. A dataset size of 2000 is used. The red vertical line $x = 0.00577$ is the performance of GPR on the same dataset.

Appendix D Description of Option Dataset

Table 3: A description of the dataset after cleaning. Each row represents the number of options/average implied volatility across different maturity ranges. Each column represents the corresponding values across different log moneyness ranges.

<div> <div>Maturity</div> <div>Log-mon</div> </div>	≤7 days	7–30 days	30–90 days	90–365 days	1–3 years
Panel A: Number of Options					
[-1.2, -0.9]	8	134	262	1114	459
(-0.9, -0.6]	26	194	417	2430	917
(-0.6, -0.3]	177	725	1421	8480	2934
(-0.3, 0]	1291	5769	11378	23659	5627
(0, 0.3]	792	4194	7435	16967	3940
Panel B: Average Implied Volatility					
[-1.2, -0.9]	2.28	1.38	0.82	0.56	0.42
(-0.9, -0.6]	2.08	1.02	0.65	0.46	0.37
(-0.6, -0.3]	1.50	0.63	0.44	0.34	0.30
(-0.3, 0]	0.56	0.31	0.25	0.24	0.23
(0, 0.3]	0.44	0.21	0.17	0.16	0.16

Appendix E Formula for Double-barrier Options

It is shown in [Kunitomo and Ikeda \(1992\)](#) that a double-barrier call option with upper (lower) bound L (U) admits the following analytical price:

$$\begin{aligned}
 V(t, S; K, T, L, U) = & S \sum_{n=-\infty}^{\infty} \left\{ \left(\frac{F^n}{E^n} \right)^{c_n} [\mathcal{N}(d_{1,n}) - \mathcal{N}(d_{2,n})] - \left(\frac{E^{n+1}}{F^n S} \right)^{c_n} [\mathcal{N}(d_{3,n}) - \mathcal{N}(d_{4,n})] \right\} \\
 & - K e^{-r\tau} \sum_{n=-\infty}^{\infty} \left\{ \left(\frac{F^n}{E^n} \right)^{c_n-2} \times [\mathcal{N}(d_{1,n} - \sigma\sqrt{\tau}) - \mathcal{N}(d_{2,n} - \sigma\sqrt{\tau})] \right. \\
 & \left. - \left(\frac{E^{n+1}}{F^n S} \right)^{c_n-2} \times [\mathcal{N}(d_{3,n} - \sigma\sqrt{\tau}) - \mathcal{N}(d_{4,n} - \sigma\sqrt{\tau})] \right\},
 \end{aligned}$$

with $c_n = \frac{2|r|}{\sigma^2} + 1$, $F = e^U$, $E = e^L$ and

$$\begin{aligned}
 d_{1,n} &= \frac{\ln(S/K) + 2n(U - L) + (r + \sigma^2/2)\tau}{\sigma\sqrt{\tau}}, \\
 d_{2,n} &= \frac{\ln(S/U) + 2n(U - L) + (r + \sigma^2/2)\tau}{\sigma\sqrt{\tau}}, \\
 d_{3,n} &= \frac{\ln(L^2/KS) - 2n(U - L) + (r + \sigma^2/2)\tau}{\sigma\sqrt{\tau}}, \\
 d_{4,n} &= \frac{\ln(L^2/US) - 2n(U - L) + (r + \sigma^2/2)\tau}{\sigma\sqrt{\tau}}.
 \end{aligned}$$